Implementation of trait-based ozone plant sensitivity in the Yale Interactive terrestrial Biosphere model v1.0 to assess global vegetation damage

Yimian Ma [1, 2], Xu Yue [3*], Stephen Sitch [4*], Nadine Unger [3], Johan Uddling [5], Lina M. Mercado [4, 6], Cheng Gong [7], Zhaozhong Feng [8], Huiyi Yang [9], Hao Zhou [1, 2], Chenguang Tian [1, 2], Yang Cao [1, 2], Yadong Lei [10], Alexander W. Cheesman [4, 11], Yansen Xu [8], Maria Carolina Duran Rojas [12]

[1] Climate Change Research Center, Institute of Atmospheric Physics, Chinese Academy of Sciences, Beijing, 100029, China
[2] University of Chinese Academy of Sciences, Beijing, 100029, China
[3] Jiangsu Key Laboratory of Atmospheric Environment Monitoring and Pollution Control, Jiangsu Collaborative Innovation Center of Atmospheric Environment and Equipment Technology, School of Environmental Science and Engineering, Nanjing University of Information Science and Technology, Nanjing, 210044, China
[4] Faculty of Environment, Science and Economy, University of Exeter, Exeter, EX4 4RJ, UK
[5] Department of Biological and Environmental Sciences, University of Gothenburg, Gothenburg, P.O. Box 461, 40530, Sweden
[6] UK Centre for Ecology and Hydrology, Benson Lane, Wallingford, OX10 8BB, UK
[7] State Key Laboratory of Atmospheric Boundary Layer Physics and Atmospheric Chemistry (LAPC), Institute of Atmospheric Physics, Chinese Academy of Sciences, Beijing, 100029, China
[8] School of Applied Meteorology, Nanjing University of Information Science and Technology, Nanjing, 210044, China
[9] Livelihoods and Institutions Department, Natural Resources Institute, University of Greenwich, Kent, ME4 4TB, UK
[10] Chinese Academy of Meteorological Sciences, Beijing, 100081, China
[11] Centre for Tropical Environmental and Sustainability Science, College of Science & Engineering, James Cook University, Cairns, Queensland, 4870 Australia
[12] College of Engineering, Mathematics, and Physical Sciences, University of Exeter, Exeter, EX4 4PY, UK

Correspondence to: Xu Yue (yuexu@nuist.edu.cn) and Stephen Sitch (S.A.Sitch@exeter.ac.uk)

Abstract

A major limitation in modeling global ozone (O_3) vegetation damage has long been the reliance on empirical O_3 sensitivity parameters derived from a limited number of species and applied at the level of plant functional types (PFTs), which ignore the large interspecific variations within the same PFT. Here, we present a major advance in large-scale assessments of O_3 plant injury by linking the trait leaf mass per area (LMA) and plant O_3 sensitivity in a broad and global perspective. Application of the new approach and a global LMA map in a dynamic global vegetation model reasonably represents the observed interspecific responses to O_3 with a unified sensitivity parameter for all plant species. Simulations suggest a contemporary global mean reduction of 4.8% in gross primary productivity by O_3, with a range of 1.1%-12.6% for varied PFTs. Hotspots with damages > 10% are found in agricultural areas in the eastern U.S., western Europe, eastern China, and India, accompanied by moderate to high levels of surface O_3. Furthermore, we simulate the distribution of plant sensitivity to O_3, which is highly linked with the inherent leaf trait trade-off strategies of plants, revealing high risks for fast-growing species with low LMA, such as crops, grasses and deciduous trees.

1. Introduction

Tropospheric ozone (O_3) has long been recognized as a hazardous pollutant for plants (Richards et al., 1958; Reich and Amundson, 1985). As a strong oxidant, O_3 can cause damage to leaf cells (Feng et al., 2014), impact stomata conductance (Buker et al., 2015), and reduce photosynthesis and biomass (Wittig et al., 2009). These negative impacts dampen global plant productivity (Ainsworth et al., 2012; Ainsworth et al., 2020) and crop yield (Tai et al., 2014; Emberson et al., 2018; Feng et al., 2022), altering multiple ecosystem functions and services across various spatiotemporal scales (Agathokleous et al., 2020; Feng et al., 2021). Thus, it is of crucial importance to quantify O_3 plant damage in global modeling and assess its coupling effects in the biosphere-atmosphere systems (Zhou et al., 2018).

To date, O_3 fumigation experiments have been conducted for various plant species. Accordingly, O_3 damage sensitivities, denoted as the Dose-Response Relationships (DRRs), were derived as the regressions between O_3 exposure metrics and the changes in biotic indicators (Mills et al., 2011). The widely-used O_3 metrics include ambient O_3 concentrations for AOT40 (Accumulated O_3 concentration above the Threshold of 40 ppbv (Fuhrer et al., 1997)), or the stomatal O_3 flux for POD_y (Phytotoxic O_3 Dose above a threshold flux of y (Buker et al., 2015)). The biotic indicators include visual leaf states, photosynthetic rate, biomass, or crop yield. Normally, the DRRs were derived for typical tree/grass species in specific regions, for example, Norway spruce, birch, and beech in Europe (Buker et al., 2015) or poplar (Shang et al., 2017) and crops (Peng et al., 2019) in East Asia.

Some assessment studies used DRRs to derive contemporary O_3 plant damage patterns at large scales. Concentration-based DRRs were widely measured and applied on the homogenized land cover, mostly for estimating crop yield loss (Feng et al., 2022; Tai et al., 2021; Hong et al., 2020). However, such DRRs do not include information about biochemical defense and stomatal regulation. In comparison, flux-based DRRs reflect a more detailed consideration in biological processes, but are limited by the application scales in both space and time (Mills et al., 2011; Mills et al., 2018b). For example, the estimate of POD_y needs a dry deposition model "DO_3SE" (Deposition of Ozone for Stomatal Exchange) (Clrtap, 2017) or an equivalent model to account for environmental constraints on plant stomatal uptake during the whole growing season. Furthermore, the application of DRRs might introduce uncertainties due to the omission of complex interactions among biotic and abiotic factors at varied spatiotemporal scales.

Alternatively, more and more mechanistic schemes were developed and implemented in dynamic global vegetation models (DGVMs) to assess the joint effects of environmental factors and O_3 on plants. Felzer et al. (2004) considered both the damaging (through AOT40) and healing (through growth) processes related to O_3 effects within the framework of Terrestrial Ecosystem Model. They further estimated the reduction of 2.6%-6.8% in the net primary productivity by O_3 pollution in U.S. during 1980-1990. Different from Felzer et al. (2004), Sitch et al. (2007) proposed a flux-based scheme linking the instantaneous POD_y with plant damage through the coupling between stomatal conductance and photosynthetic rate. Implementing this scheme into the vegetation model of YIBs, Yue and Unger (2015) predicted a range of 2%-5% reduction in global gross primary productivity (GPP) taking into account the low to high O_3 sensitivities for each vegetation type. Lombardozzi et al. (2015) collected hundreds of measurements and derived the decoupled responses on stomatal conductance and photosynthesis for the same O_3 uptake fluxes. They further implemented the separate response relationships into the Community Land Model and estimated a reduction of 8%-12% in GPP by O_3 at present day. Coupling these schemes with earth system models, studies have assessed interactive O_3 impacts on the carbon sink (Oliver et al., 2018; Yue and Unger, 2018), global warming (Sitch et al., 2007), and air pollution (Zhou et al., 2018; Gong et al., 2020; Gong et al., 2021; Zhu et al., 2022).

Although different schemes considered varied physical processes (Ollinger et al., 1997; Felzer et al., 2004; Sitch et al., 2007; Felzer et al., 2009; Lombardozzi et al., 2015; Oliver et al., 2018), they followed the same principle that different O_3 sensitivities should be applied for varied plant functional types (PFTs), as revealed by many measurements in the past four decades (Buker et al., 2015; Mills et al., 2018b) (Table S1). Generally, needleleaf trees, deciduous woody plants, and crop species show ascending sensitivities to O_3 (Reich and Amundson, 1985; Davison and Barnes, 1998; Buker et al., 2015). But the cause of such variation is not fully understood and thus has not been uniformly described in vegetation models (Massman et al., 2000; Tiwari et al., 2016). As a result, all large-scale assessments of O_3 vegetation damage had to rely on a PFT-based range of sensitivity parameters derived from a limited number of plant species and attempted to envelop the range of O_3 impacts by assuming all species within a PFT are either "high" or "low" sensitive to O_3. For example, Felzer et al. (2004) defined empirical sensitivity coefficients for three major plants including deciduous trees, coniferous trees, and crops. In Sitch et al. (2007), the sensitivity coefficients were defined separately for five PFTs with high/low ranges calibrated by DRRs of typical species. These synthesized assumptions cannot resolve the intra-PFT variations in the O_3 sensitivity and thus may cause large uncertainties in regional to global assessments.

Recent observations revealed a uniform plant sensitivity to O_3 if stomatal O_3 flux was expressed based on a leaf mass rather than leaf area basis (Li et al., 2016; Feng et al., 2018; Li et al., 2022). The trait of leaf mass per area (LMA) is an important metric linking leaf area to mass. In a comparative study with 21 woody species (Li et al., 2016) and a meta-analysis of available experimental data (Feng et al., 2018), the DRR showed convergent O_3 sensitivities for conifer and broadleaf trees if the area-based stomatal uptake was converted to the mass-based flux with LMA. This is likely related to the diluting effect of thicker leaves, which normally have stronger defenses against O_3 in their cross-section. Nowadays, a large number of trait observations have been synthesized by global networks (Gallagher et al., 2020). The TRY initiative (Kattge et al., 2011) was one of the most influential datasets with 2.3 billion trait data by the year 2021. Based on the TRY dataset, global LMA was estimated with upscaling techniques such as Bayesian modeling (Butler et al., 2017) (thereafter B2017) or the random forest model (Moreno-Martinez et al., 2018) (thereafter M2018). These advances in the retrieval of LMA provide the possibility to depict more accurate O_3 vegetation damage at the global scale.

Here, we present a major advance in large-scale assessments of O_3 plant damage using a trait-based approach. We implement LMA into a stomatal flux-based O_3 damage framework aiming at a unified representation of plant O_3 sensitivities over the global grids. We couple this new approach to the Yale Interactive terrestrial Biosphere (YIBs) model (Yue and Unger, 2015) and evaluate the derived O_3 sensitivities against observations. We further assess contemporary O_3 impacts on global GPP in combination with the recently developed LMA datasets (Butler et al., 2017; Moreno-Martinez et al., 2018;

Gallagher et al., 2020) (Fig. 1a) and the multi-model ensemble mean surface O_3 concentrations (Fig. 1b). The updated risk map for O_3 vegetation damage is used to identify the regions and vegetation types most at risk to O_3.

2. Scheme development and calibration

2.1 The trait-based O_3 vegetation damage scheme

We develop the new scheme based on the Sitch et al. (2007) (hereafter S2007) framework for transient O_3 damage calculation. In the original S2007 scheme, the undamaged fraction F for net photosynthetic rate is dependent on the excessive area-based stomatal O_3 flux, which is calculated as the difference between f_{O3} and PFT-specific area-based threshold y, and modulated by the sensitivity parameter a_{PFT}:

$$F = 1 - a_{PFT} \times max\{f_{O3} - y, 0\} \tag{1}$$

where a_{PFT} is calibrated and varies among PFTs with a typical range from “low” to “high” values indicating uncertainties of plant species within the same PFT. The stomatal O_3 flux f_{O3} (nmol m^{-2} s^{-1}) is calculated as:

$$f_{O3} = \frac{[O_3]}{r + \left[\frac{k_{O3}}{g_p \times F}\right]} \tag{2}$$

where $[O_3]$ is the O_3 concentration at the reference level (nmol m^{-3}), r is the aerodynamic and boundary layer resistance between leaf surface and reference level (s m^{-1}). k_{O3} setting to 1.67 represents the ratio of leaf resistance for O_3 to that for water vapor. g_p represents potential stomata conductance for H_2O (m s^{-1}).

Studies suggested that LMA could be used to unify the area-based plant sensitivities to O_3 (Li et al., 2016; Feng et al., 2018), resulting in a constant mass-based parameter a independent of plant species and PFTs:

$$a = a_{PFT} \times LMA \tag{3}$$

Here, we convert the area-based O_3 stomatal flux expression in Equation (1) to a mass-based flux as follows:

$$F = 1 - a \times \max\left\{\frac{f_{O3}}{LMA} - x, 0\right\} \tag{4}$$

where the new sensitivity parameter a is a cross-species constant (nmol^{-1} s g); *LMA* is leaf mass per area (g m^{-2}); the flux threshold is replaced by a mass-based value of x (nmol g^{-1} s^{-1}) (Feng et al., 2018). Equations (2) and (4) can form a quadratic equation. The *F* can be derived at each timestep (i.e. hourly) and applied to net photosynthetic rate and stomatal conductance to calculate the O_3-induced damages. The updated LMA-based framework (YIBs-LMA) reduces the number of O_3 sensitivity parameters from three for each PFT (Sitch et al., 2007) in S2007 to a single parameter a for all PFTs. For YIBs-LMA framework, the default value of the x threshold in Equation (4) is set to 0.019 nmol g^{-1} s^{-1} as recommended by Feng et al. (2018).

2.2 Dose-response relationship (DRR)

We compare the simulated and observed sensitivities to O_3 so as to calibrate the LMA-based scheme. In field experiments, DRR is used to quantify species-specific damage by O_3 with a generic format as follows:

$$R = 100 + S_O \times \phi_{O3} \tag{5}$$

where *R* (%) is the relative percentage of a biotic indicator (such as biomass or yield) after and before O_3 damage; ϕ_{O3} is an area-based O_3 metric (e.g., POD_y measured in sunlit leaves at the top of canopy); S_O (usually negative) is the observed sensitivity derived as the slope of linear relationship between *R* and ϕ_{O3}. We collected S_O from DRRs with conventional criteria (typically $POD_{y=1}$ for natural PFTs and $POD_{y=6}$ for crops as dose metrics (Clrtap, 2017); the biotic indicators include the relative biomass for natural PFTs and relative yield for crops) among plant species from International Cooperative Programme on Effects of Air Pollution on Natural Vegetation and Crops (CLRTAP) (Clrtap, 2017) and multiple literature sources (Table S1). Such observations are used to calibrate the LMA-based scheme.

As a comparison with observations, we calculate annual relative GPP percentage (R_{GPP}, %) and POD_y of sunlit leaves in the first canopy layer (mmol m^{-2} year^{-1}, based on per leaf area) from the vegetation model to derive the slopes (S_S) of simulated DRRs. Here, POD_y is a diagnostic variable calculated as:

$$POD_y = \int \max\{f_{O3} - y, 0\} \tag{6}$$

where f_{O3} represents the stomatal O_3 flux under instant O_3 stimulus at each timestep, which can be calculated following Equation (2) at the leaf level; y is the prescribed critical level (1 nmol m^{-2} s^{-1} for natural or 6 nmol m^{-2} s^{-1} for crop species (Clrtap, 2017)). Excessive O_3 flux above y is accumulated for the sunlit leaves of the top canopy layer and over the growing season to derive the POD_y. Simulated S_S is calculated as the slope of the regression between simulated R_{GPP} (%) and POD_y at the PFT level. Only the dominant PFT in each grid is considered for the estimate of S_S at both PFT-level or gridded analyses.

Similarly, mass-based POD_x is derived from O_3-impacted f_{O3} (nmol m^{-2} s^{-1}) in Equation (2), together with gridded LMA (g m^{-2}) and mass-based threshold x (nmol g^{-1} s^{-1}) as:

$$POD_x = \int \left(\frac{f_{O3}}{LMA} - x\right) \tag{7}$$

2.3 Simulations and calibrations

We perform two groups of supporting experiments (Table 1). The first group explores modeling uncertainties associated with the mass-based framework: (1) YIBs-LMA_B2017 replaces the default LMA map of M2018 (Moreno-Martinez et al., 2018) with B2017 (Butler et al., 2017). (2) YIBs-LMA_PFT applies PFT-specific LMA values (Table S2) for each PFT without considering global LMA geo-gradient. (3) YIBs-LMA_T replaces the default threshold of x=0.019 nmol g^{-1} s^{-1} with x =0.006 nmol g^{-1} s^{-1}, which is an alternative parameter suggested by observations (Feng et al., 2018). The second group of supporting experiments explores the differences between mass-based and S2007 area-based frameworks. Typically, S2007 has a "low to high" a_{PFT} range for each PFT. Here, a mean sensitivity parameterization of S2007 (YIBs-S2007_adj) is re-calibrated according to S_O in Table S1.

For all supporting experiments, the parameter a for YIBs-LMA or the eight mean a_{PFT} for YIBs-S2007_adj are derived with the optimal 1:1 fitting between S_S and S_O to minimize the possible biases (Tables 2 and S3-S6). The basic method for calibration is feeding the model with series values of a or a_{PFT} until the predicted O_3 damage matches observations with the lowest normalized mean biases (NMB). For all LMA-based experiments, S_S from varied PFTs were grouped for the calibration of a, while for a_{PFT} in YIBs-S2007_adj, each a_{PFT} is determined individually by matching simulated S_S with S_O. Since

S_O are available only for six out of the eight YIBs PFTs, including EBF, NF, DBF, C_3 grass, C_4 grass, and crop (Table S1), S_O of these PFTs are used for calibration. All runs are summarized in Table 1.

2.4 YIBs model and forcing data

In this study, all O_3 vegetation damage schemes are implemented in the YIBs model (Yue and Unger, 2015), which is a process-based dynamic global vegetation model incorporated with well-established carbon, energy, and water interactive schemes. The model applies the same PFT classifications as the Community Land Model (Bonan et al., 2003) (Fig. S1). Eight PFTs are employed including evergreen broadleaf forest (EBF), needleleaf forest (NF), deciduous broadleaf forest (DBF), cold shrub (C_SHR), arid shrubland (A_SHR), C_3 grassland (C3_GRA), C_4 grassland (C4_GRA), and cropland (CRO) (Fig. S1). For each PFT, phenology is well-evaluated (Yue and Unger, 2015) to generate a reliable growing season, which is crucial for the simulation of stomatal O_3 uptake (Anav et al., 2018). Photosynthesis and stomatal processes are calculated using Farquhar et al. and Ball-Berry algorithms (Farquhar et al., 1980; Ball et al., 1987), respectively. Leaf area index (LAI) and tree height are predicted dynamically based on vegetation carbon allocation. The YIBs model has joined the multi-model ensemble project TRENDY and showed reasonable performance in the simulations of global biomass, GPP, LAI, net ecosystem exchange, and soil carbon relative to observations (Friedlingstein et al., 2020). Key plant biogeochemical parameters of the YIBs model are adjusted for this research (Table S7).

The hourly modern-era retrospective analysis for research and applications version 2 (MERRA2) climate reanalyses (Gelaro et al., 2017) are used to drive the YIBs model. The gridded LMA required for the main mass-based simulation is derived from Moreno-Martinez et al. (2018) (M2018), which shows the highest value of >150 g m^{-2} for needleleaf forest at high latitudes while low values of ~40 g m^{-2} for grassland and cropland (Fig. 1a and Fig. S1). Grids with missing LMA data are filled with the mean of the corresponding PFT. Contemporary O_3 concentration fields in the year 2010 from the multi-model mean in Task Force on Hemispheric Transport of Air Pollutants (TF-HTAP) experiments (Turnock et al., 2018) (Fig. 1b) are used as forcing data. The original monthly O_3 data are downscaled to hourly using the diurnal cycle predicted by the chemistry-climate-carbon fully coupled model ModelE2-YIBs (Yue and Unger, 2015).

Generally, areas of severe O_3 pollution are found in the mid-latitudes of the Northern Hemisphere with highest annual average O_3 concentration of over 40 ppbv in East Asia. All data are interpolated to the spatial resolution of $1^o\times1^o$.

3. Results

3.1 Comparison of simulated sensitivities with observations

Simulated relative GPP percentage (R_{GPP}) at global grids were sorted by dominant PFTs (Fig. S1) and plotted against area-based accumulated phytotoxic O_3 dose above a threshold y nmol m^{-2} s^{-1} ($POD_{y=1}$) at the corresponding grids (Fig. 2). The DRR shows varied slopes among different PFTs, resulting in a coefficient of determination (R^2) around 0.54 for all PFTs (Figs 2a-2c). We further calculated the mass-based accumulated phytotoxic O_3 dose above a threshold of 0.019 nmol g s^{-1} ($POD_{x=0.019}$) and compared it with R_{GPP}. The updated DRR showed convergent slopes and reached a high R^2 of 0.77 across all PFTs (Figs 2d-2f), suggesting that the mass-based scheme could better unify O_3 sensitivities among different PFTs.

We then calibrated the single, best-fit a value for the YIBs-LMA framework by minimizing the absolute difference between simulated (S_S) and observed (S_O) slopes of O_3 DRR for all PFTs. With different a parameters, the YIBs-LMA framework yielded considerably high R^2 of ~1.0 but varied biases between simulated and observed O_3 impacts across PFTs (Fig. 3). Both the 1:1 fitting and the lowest bias between S_S and S_O were achieved with an optimal a =3.5 $nmol^{-1}$ s g (Fig. 3c). Notably, such calibration of a is robust under different O_3 fields (see Fig. S2). Consistent with observations, YIBs-LMA with this optimal a parameter simulated low S_S of -0.18% and -0.36% per mmol m^{-2} $year^{-1}$ of $POD_{y=1}$ for evergreen broadleaf forest and needleleaf forest, respectively (Figs 4a, b), median S_S from -0.53% per mmol m^{-2} $year^{-1}$ for arid shrubland (Fig. 4e), and high S_S from -0.64% to -1.04% per mmol m^{-2} $year^{-1}$ for deciduous broadleaf forest, C_3/C_4 grassland, cropland and cold shrubland (-3.28% for crops with $POD_{y=6}$, Figs 4c-d, 4f-h).

3.2 Global map of O_3 vegetation damage

We estimated contemporary GPP reductions induced by O_3 with the global concentrations of surface O_3 (Fig. 1b) in the year 2010. The YIBs-LMA framework using an increase of *a* parameter yielded an almost linear enhancement of global GPP reduction (Fig. S3) with consistent spatial distributions (Fig. S4). The simulation with the optimal $a = 3.5$ nmol^{-1} s g predicted a global GPP reduction of 4.8% (Fig. 5a), which was similar to the value estimated with the area-based S2007 scheme (YIBs-S2007_adj, Table 1). Large reductions of >10% were predicted over the eastern U.S., western Europe, eastern China, and India (Fig. 5a). Hotspots were mainly located in cropland and agricultural areas mixed with deciduous broadleaf forest or grassland, accompanied by moderate to high levels of surface O_3. Few discrepancies between the damage maps of YIBs-LMA and YIBs-S007_adj were found (Fig. 5b and Fig. S5), even though the number of parameters was greatly reduced in the YIBs-LMA scheme.

For YIBs-LMA, PFTs with low LMA such as cropland, grassland, and deciduous broadleaf forest account for 73.3 Pg C yr^{-1} (50.0%) of the global GPP (Table S8). However, these PFTs contributed to a total GPP reduction of 5.4 Pg C yr^{-1} (75.5% of total GPP loss) by O_3 damage. In contrast, evergreen broadleaf and needleleaf forests with high LMA accounted for 48.8 Pg C yr^{-1} (33.0%) of total GPP but yielded only a reduction of 0.75 Pg C yr^{-1} (10.5% of total GPP loss). Differences in GPP percentage losses were in part associated with the global pattern of O_3 concentrations, which were usually higher over mid-latitudes with populated cities and dense crop plantations (Fig. 1b). However, the differences in LMA and simulated O_3 sensitivities of these PFTs also made important contributions to such discrepancies in GPP damage.

3.3 Uncertainties of the LMA-based scheme

We quantified the uncertainties in the LMA-based scheme by comparing simulated GPP damages among different experiments (Table 1). The experiment with the alternative LMA map of B2017 (Fig. S6) showed similar spatial patterns but a slightly enhanced GPP reduction of 5.3% (Fig. 6a) compared to the simulations using LMA map of M2018 (Fig. 5a). The B2017 map contains much LMA data than M2018 (~40%), leading to unexpected high O_3 threats over the tundra in the Arctic (Fig. S7). Another experiment using PFT-specific LMA estimated a global GPP reduction of 4.6% (Fig. 6b) with a consistent spatial pattern as the prediction in YIBs-LMA, suggesting that the PFT-level LMA can be used in case of the lack of regional LMA data. The third experiment with an alternative threshold flux (Feng et al., 2018) of 0.006 nmol g^{-1} s^{-1} estimated a high GPP reduction of 6.5% (Fig. 6c) due to the overestimations of O_3 sensitivities for some tree PFTs (Fig. 7). The fourth run, YIBs-S2007_adj, predicted a similar global GPP damage of 4.8% as the YIBs-LMA run with a high spatial correlation coefficient of 0.98 (Fig. 6d). Such good consistency is mainly due to the application of recalibrated PFT-level sensitivities in YIBs-S2007_adj. Finally, we tested a new calibration excluding CRO, the PFT that contributed the most to the calibration biases (shown as orange dashed lines in Fig. S8). The results gave an optimal *a* of 3.2, with global damage of 4.5%. All sensitivity experiments achieved consistent results as the YIBs-LMA simulation with damages ranging from 4.5% to 6.5% and spatial correlation coefficients larger than 0.94.

4. Discussion

4.1 Mechanisms behind the LMA-based approach

In recent decades, the plant science community examined how traits could be used to differentiate and predict the function of plant species (Reich et al., 1997; Reich et al., 1999). LMA, related to leaf density and thickness, is a key trait reflecting many aspects of leaf function (Reich et al., 1998). In the field of O_3 phytotoxicology, experiments have revealed plants with high LMA usually have thick leaves with physical and chemical defenses (Poorter et al., 2009), which can strengthen their resistance to O_3 (Li et al., 2016; Feng et al., 2018). On the contrary, plants with low LMA normally have thin leaves which are likely to be less O_3-tolerant (Li et al., 2016; Feng et al., 2018). Moreover, it seems plausible that the oxidative stress caused by a given amount of stomatal O_3 flux per unit leaf area would be distributed over a larger leaf mass, and hence diluted, in a leaf with high LMA. Such an LMA-O_3 sensitivity relationship can be well reproduced by our LMA-based model (Figs 8a and 8b). Below we explore the linkage between O_3 plant sensitivities and the mutual adaptation of growth strategies and leaf morphology with plant leaf trade-off theory (Reich et al., 1999; Shipley et al., 2006).

In the natural world, plants often adapt to maximize carbon uptake under prevailing conditions (Reich et al., 1998; Shipley et al., 2006). To make full use of resources in the growing season, leaves under varied living conditions choose either fast photosynthetic rates (fast-growing deciduous types) or long photosynthesis duration (slow-growing evergreen types) with compatible leaf structures (Reich, 2014; Diaz et al., 2016). The former species expand leaf area (low LMA) to maximize light interception while the latter species produce thick and mechanically strong leaves (high LMA) with ample resistant substances for durable utilization (Poorter et al., 2009) in resource-limited and/or environment-stressed habitats (Wright et al., 2002). As a side effect of such leaf trade-offs, deciduous plants with their high rates of photosynthesis, associated large stomatal conductance (Davison and Barnes, 1998; Henry et al., 2019), and less total defense capacity through the leaf profile (Poorter et al., 2009), are highly O_3 sensitive (Mode1 in Fig. 9). In contrast, the moderate photosynthesis, relatively low maximum stomatal conductance (Davison and Barnes, 1998; Henry et al., 2019), and reinforced dense leaves (Poorter et al., 2009) lead to low sensitivity for evergreen plants (Mode2 in Fig. 9). Therefore, in our modeling practice, the mass-based O_3 gas exchange algorithm can be regarded as taking into account several interrelated factors such as growth-driven gas exchange requirements, gas path length, and biochemical reserves, in a unified, simplified and effective manner via LMA.

4.2 Implication of potential risks for fast-growing plants

Our new approach reflected the general experimental findings that deciduous plants are much more vulnerable to O_3 than evergreen species (Li et al., 2017; Feng et al., 2018), and in turn within a PFT, early-successional/pioneers with low LMA are likely more vulnerable than late-successional/canopy trees with high LMA (Fyllas et al., 2012). This law has been neglected in previous modeling studies due to the dependence on the limited observed data used for PFT-specific tuning. Our LMA-based approach bridges this gap through grid-based parameterization, and in addition, our data-model integration specifically emphasizes the broad high risks for fast-growing plants, especially for crops. Among PFTs, crops may endure the largest O_3 threats (Davison and Barnes, 1998; Feng et al., 2021; Mukherjee et al., 2021) because they are artificially bred with high photosynthetic capacities (Richards, 2000), stomatal conductance, generally low LMA (Bertin and Gary, 1998; Wang and Shangguan, 2010; Wu et al., 2018; Li et al., 2018) (roughly 30-60 g m^{-2}), and cultivated in populated regions with high ambient O_3 concentrations. Modern technology aims to promote crop yield (Herdt, 2005), but this can potentially elevate crop sensitivities to O_3 (Biswas et al., 2008; Biswas et al., 2013). This study estimated the highest annual mean GPP damage for crop, 12.6%, which is at the high end of the 4.4-12.4% of the O_3-induced yield loss estimated for global modeling of soybean, wheat, rice, and maize (Mills et al., 2018a). Furthermore, human-induced land use activities may also increase O_3 damage risks. The global demand for food and commodities leads to the conversion of natural forests to irrigated croplands, grazing pastures, and economical-tree plantations (Curtis et al., 2018; Zalles et al., 2021). Meanwhile, the urgent actions to combat climate change promote large-scale afforestation and reforestation (Cook-Patton et al., 2020). These land use changes with fast-growing plant species may increase the risks of terrestrial ecosystems to surface O_3.

4.3 Advances in the global O_3 damage assessment

For the first time, we implemented plant trait LMA into a process-based O_3 impact modeling scheme and obtained reasonable interspecific and inter-PFT O_3 responses supported by observations. The similarity between YIBs-S2007 and YIBs-LMA shown in Fig. 5 revealed an advance in the modeling strategy. Simulated O_3 damage in YIBs-S2007 is based on the PFT-level calibrations that tuned sensitivity parameters of each PFT with observed DRRs. Such refinement is a data-driven approach without clear physical reasons. Instead, the YIBs-LMA framework converts the area-based responses to mass-based ones and achieves better unification in O_3 sensitivities among different PFTs. In this algorithm, the O_3 damage efficiency is inversely related to plant LMA, which influences both the O_3 uptake potential and the detoxification capability of the vegetation. The similarity in the global assessment of O_3 vegetation damage between YIBs-S2007 and YIBs-LMA further demonstrated the physical validity of LMA-based scheme in the Earth system modeling, because the independent LMA map was applied in the latter approach.

In addition to the advance in physical mechanisms, the LMA-based approach improves global O_3 damage assessments in the following aspects. First, it significantly reduces the number of required key parameters. To account for interspecific sensitivities, many schemes have to define PFT-level parameters to capture the ranges of plant responses (Sitch et al., 2007; Felzer et al., 2009; Lombardozzi et al., 2015). As a result, those schemes rely on dozens of parameters which increases the uncertainties of modeling and the difficulties for model calibration. The LMA-based approach requires the calibration of one single parameter *a*, largely facilitating its application across different vegetation models. Second, the new approach accounts for the continuous spectrum of O_3 sensitivities. Previous studies usually categorized species into groups of low or high O_3 sensitivity, depending on very limited data from O_3 exposure experiments. As a result, gridcells for a specific PFT share the same sensitivities regardless of their geographic locations and ecosystem characteristics. In reality, there are hundreds and thousands of plant species in each PFT and they usually have large variations in biophysical parameters including LMA and O_3 sensitivities. The LMA-based approach takes advantage of the newly revealed unifying concept in O_3 sensitivity (Li et al., 2016; Feng et al., 2018; Li et al., 2022) and the recent development in a trait-based LMA global map (Fig. 1a). Such configurations present a spectrum of gridded O_3 sensitivities (Fig. 8a) following the variations of LMA distribution.

4.4 Outlook for future modeling

In nature, all aspects of plant physiochemical processes, such as growth, development, reproduction, and defense, are influenced by abiotic factors like water availability, temperature, CO_2 concentration, and light resources (Kochhar and Gujral, 2020). In our modeling, the cumulative O_3 fluxes are based on dynamic plant simulations with well-established DGVM to calculate the effects of these abiotic factors. LMA is considered as a factor representing the vulnerability of each species, by which divergent responses to the same O_3 stomatal dose can be further differentiated. In fact, many other key variables in DGVMs, for example, leaf photosynthetic traits (V_{cmax} and J_{max}), nutrient traits (leaf nitrogen and phosphorus), morphological traits (leaf thickness and size), and phenology-related traits (leaf life span) are all more or less interlinked with LMA (Walker et al., 2014). There are some generic regression relationships between them. In addition, efforts are being made to directly predict key traits, including LMA, through environmental factors. As a result, considerable improvements can be made in the direction of trait-flexible modeling within the existing DGVM frameworks. Our study demonstrates the validity of LMA-based approach for the O_3 plant damage modeling.

Although we used the most advanced LMA integrated from available observations, this dataset was developed based on static global grids and revealed the mean state for each pixel. In reality, LMA can vary with biotic/abiotic factors like leaf position in the canopy (Keenan and Niinemets, 2017), phenology, plant health, living environment (Fritz et al., 2018), and climate (Wright et al., 2005; Cui et al., 2020). Even long-term exposure to O_3 can alter leaf morphological characteristics and LMA (Li et al., 2017). In future studies, simulations from local to global scales could implement the spatiotemporal variations in LMA taking into account the demographic information and environmental forcings. We expect a breakthrough in the calculation of reliable LMA to achieve fully dynamic predictions of O_3 plant damage in Earth System Modeling, thus facilitating the research of plant response and adaption in changing environments.

Code availability

The codes of YIBs model with LMA-based O_3 damaging scheme are shared at https://zenodo.org/record/6348731.

Data availability

Results of all simulations (listed in Table 1) are available upon request. Data for Figures in the main article are shared at https://zenodo.org/record/6348731. The global maps of specific leaf area (SLA) to derive LMA for M2018 and B2017 are from https://www.try-db.org/TryWeb/Data.php#59 and https://github.com/abhirupdatta/global_maps_of_plant_traits, respectively. Monthly O_3 data is from https://doi.org/10.5194/acp-18-8953-2018. Calibration data are summarized in Table S1.

Author Contributions

X.Y., S.S. and N.U. designed the research, Y.M.M. performed modeling, data analyses, virtualization and wrote the draft. J.U, L.M., Z.Z.F, and A.W.C advised on concepts and methods. C.G. helped write draft. H.Y.Y., M.C.D.R helped with coding. H.Z., C.G.T., Y.C., Y.D.L., and Y.S.X. helped with data collection. All authors commented and revised the manuscript.

Competing interests

The authors declare no conflict of interests.

Financial support

Xu Yue acknowledges funding supports from the National Natural Science Foundation of China (grant no. 42293323) and Jiangsu Science Fund for Distinguished Young Scholars (grant no. BK20200040). Yimian Ma acknowledges financial support from China Scholarship Council (CSC no. 201804910712). Johan Uddling acknowledges the strategic research area Biodiversity and Ecosystems in a Changing Climate, BECC. SS, NU, LM, AC were supported by NERC funding (NE/R001812/1).

References

Agathokleous, E., Feng, Z., Oksanen, E., Sicard, P., Wang, Q., Saitanis, C. J., Araminiene, V., Blande, J. D., Hayes, F., Calatayud, V., Domingos, M., Veresoglou, S. D., Penuelas, J., Wardle, D. A., De Marco, A., Li, Z., Harmens, H., Yuan, X., Vitale, M., and Paoletti, E.: Ozone affects plant, insect, and soil microbial communities: A threat to terrestrial ecosystems and biodiversity, Sci Adv, 6, 10.1126/sciadv.abc1176, 2020.

Ainsworth, E. A., Lemonnier, P., and Wedow, J. M.: The influence of rising tropospheric carbon dioxide and ozone on plant productivity, Plant Biology, 22, 5-11, 10.1111/plb.12973, 2020.

Ainsworth, E. A., Yendrek, C. R., Sitch, S., Collins, W. J., and Emberson, L. D.: The Effects of Tropospheric Ozone on Net Primary Productivity and Implications for Climate Change, Annu Rev Plant Biol, 63, 637-661, 10.1146/Annurev-Arplant-042110-103829, 2012.

Anav, A., Liu, Q., De Marco, A., Proietti, C., Savi, F., Paoletti, E., and Piao, S.: The role of plant phenology in stomatal ozone flux modeling, Global Change Biol, 24, 235-248, 10.1111/gcb.13823, 2018.

Ball, J. T., Woodrow, I. E., and Berry, J. A.: A model predicting stomatal conductance and its contribution to the control of photosynthesis under different environmental conditions, Progress in Photosynthesis Research: Viith International Congress on Photosynthesis, 10.1007/978-94-017-0519-6_48, 1987.

Bertin, N. and Gary, C.: Short and long term fluctuations of the leaf mass per area of tomato plants - Implications for growth models, Ann Bot-London, 82, 71-81, DOI 10.1006/anbo.1998.0647, 1998.

Biswas, D. K., Xu, H., Li, Y. G., Ma, B. L., and Jiang, G. M.: Modification of photosynthesis and growth responses to elevated CO2 by ozone in two cultivars of winter wheat with different years of release, J Exp Bot, 64, 1485-1496, 10.1093/jxb/ert005, 2013.

Biswas, D. K., Xu, H., Li, Y. G., Sun, J. Z., Wang, X. Z., Han, X. G., and Jiang, G. M.: Genotypic differences in leaf biochemical, physiological and growth responses to ozone in 20 winter wheat cultivars released over the past 60 years, Global Change Biol, 14, 46-59, 10.1111/j.1365-2486.2007.01477.x, 2008.

Bonan, G. B., Levis, S., Sitch, S., Vertenstein, M., and Oleson, K. W.: A dynamic global vegetation model for use with climate models: concepts and description of simulated vegetation dynamics, Global Change Biol, 9, 1543-1566, 10.1046/J.1365-2486.2003.00681.X, 2003.

Buker, P., Feng, Z., Uddling, J., Briolat, A., Alonso, R., Braun, S., Elvira, S., Gerosa, G., Karlsson, P. E., Le Thiec, D., Marzuoli, R., Mills, G., Oksanen, E., Wieser, G., Wilkinson, M., and Emberson, L. D.: New flux based dose-response relationships for ozone for European forest tree species, Environ Pollut, 206, 163-174, 10.1016/j.envpol.2015.06.033, 2015.

Butler, E. E., Datta, A., Flores-Moreno, H., Chen, M., Wythers, K. R., Fazayeli, F., Banerjee, A., Atkin, O. K., Kattge, J., Amiaud, B., Blonder, B., Boenisch, G., Bond-Lamberty, B., Brown, K. A., Byun, C., Campetella, G., Cerabolini, B. E. L., Cornelissen, J. H. C., Craine, J. M., Craven, D., de Vries, F. T., Diaz, S., Domingues, T. F., Forey, E., Gonzalez-Melo, A., Gross, N., Han, W., Hattingh, W. N., Hickler, T., Jansen, S., Kramer, K., Kraft, N. J. B., Kurokawa, H., Laughlin, D. C., Meir, P., Minden, V., Niinemets, U., Onoda, Y., Penuelas, J., Read, Q., Sack, L., Schamp, B., Soudzilovskaia, N. A., Spasojevic, M. J., Sosinski, E., Thornton, P. E., Valladares, F., van Bodegom, P. M., Williams, M., Wirth, C., and Reich, P. B.: Mapping local and global variability in plant trait distributions, Proc Natl Acad Sci U S A, 114, E10937-E10946, 10.1073/pnas.1708984114, 2017.

CLRTAP: The UNECE Convention on Long-range Transboundary Air Pollution, Manual on Methodologies and Criteria for Modelling and Mapping Critical Loads and Levels and Air Pollution Effects, Risks and Trends: Chapter III Mapping Critical Levels for Vegetation, 2017.

Cook-Patton, S. C., Leavitt, S. M., Gibbs, D., Harris, N. L., Lister, K., Anderson-Teixeira, K. J., Briggs, R. D., Chazdon, R. L., Crowther, T. W., Ellis, P. W., Griscom, H. P., Herrmann, V., Holl, K. D., Houghton, R. A., Larrosa, C., Lomax, G., Lucas, R., Madsen, P., Malhi, Y., Paquette, A., Parker, J. D., Paul, K., Routh, D., Roxburgh, S., Saatchi, S., van den Hoogen, J., Walker, W. S., Wheeler, C. E., Wood, S. A., Xu, L., and Griscom, B. W.: Mapping carbon accumulation potential from global natural forest regrowth, Nature, 585, 545-550, 10.1038/s41586-020-2686-x, 2020.

Cui, E., Weng, E., Yan, E., and Xia, J.: Robust leaf trait relationships across species under global environmental changes, Nat Commun, 11, 2999, 10.1038/s41467-020-16839-9, 2020.

Curtis, P. G., Slay, C. M., Harris, N. L., Tyukavina, A., and Hansen, M. C.: Classifying drivers of global forest loss, Science, 361, 1108-1111, 10.1126/science.aau3445, 2018.

Davison, A. W. and Barnes, J. D.: Effects of ozone on wild plants, New Phytol, 139, 135-151, https://doi.org/10.1046/j.1469-8137.1998.00177.x, 1998.

Diaz, S., Kattge, J., Cornelissen, J. H., Wright, I. J., Lavorel, S., Dray, S., Reu, B., Kleyer, M., Wirth, C., Prentice, I. C., Garnier, E., Bonisch, G., Westoby, M., Poorter, H., Reich, P. B., Moles, A. T., Dickie, J., Gillison, A. N., Zanne, A. E., Chave, J., Wright, S. J., Sheremet'ev, S. N., Jactel, H., Baraloto, C., Cerabolini, B., Pierce, S., Shipley, B., Kirkup, D., Casanoves, F., Joswig, J. S., Gunther, A., Falczuk, V., Ruger, N., Mahecha, M. D., and Gorne, L. D.: The global spectrum of plant form and function, Nature, 529, 167-171, 10.1038/nature16489, 2016.

Emberson, L. D., Pleijel, H., Ainsworth, E. A., van den Berg, M., Ren, W., Osborne, S., Mills, G., Pandey, D., Dentener, F., Buker, P., Ewert, F., Koeble, R., and Van Dingenen, R.: Ozone effects on crops and consideration in crop models, Eur J Agron, 100, 19-34, 10.1016/j.eja.2018.06.002, 2018.

Farquhar, G. D., Caemmerer, S. V., and Berry, J. A.: A biochemical-model of photosynthetic CO_2 assimilation in leaves of C3 Species, Planta, 149, 78-90, 10.1007/Bf00386231, 1980.

Felzer, B., Kicklighter, D., Melillo, J., Wang, C., Zhuang, Q., and Prinn, R.: Effects of ozone on net primary production and carbon sequestration in the conterminous United States using a biogeochemistry model, Tellus B, 56, 230-248, https://doi.org/10.1111/j.1600-0889.2004.00097.x, 2004.

Felzer, B. S., Cronin, T. W., Melillo, J. M., Kicklighter, D. W., and Schlosser, C. A.: Importance of carbon-nitrogen interactions and ozone on ecosystem hydrology during the 21st century, J. Geophys. Res., 114, G01020, 10.1029/2008jg000826, 2009.

Feng, Z., Xu, Y., Kobayashi, K., Dai, L., Zhang, T., Agathokleous, E., Calatayud, V., Paoletti, E., Mukherjee, A., Agrawal, M., Park, R. J., Oak, Y. J., and Yue, X.: Ozone pollution threatens the production of major staple crops in East Asia, Nature Food, 3, 47-56, 10.1038/s43016-021-00422-6, 2022.

Feng, Z., Agathokleous, E., Yue, X., Oksanen, E., Paoletti, E., Sase, H., Gandin, A., Koike, T., Calatayud, V., Yuan, X., Liu, X., De Marco, A., Jolivet, Y., Kontunen-Soppela, S., Hoshika, Y., Saji, H., Li, P., Li, Z., Watanabe, M., and Kobayashi, K.: Emerging challenges of ozone impacts on asian plants: actions are needed to protect ecosystem health, Ecosystem Health and Sustainability, 7, 1911602, 10.1080/20964129.2021.1911602, 2021.

Feng, Z. Z., Sun, J. S., Wan, W. X., Hu, E. Z., and Calatayud, V.: Evidence of widespread ozone-induced visible injury on plants in Beijing, China, Environ Pollut, 193, 296-301, 10.1016/j.envpol.2014.06.004, 2014.

Feng, Z. Z., Buker, P., Pleijel, H., Emberson, L., Karlsson, P. E., and Uddling, J.: A unifying explanation for variation in ozone sensitivity among woody plants, Glob. Change Biol., 24, 78-84, 10.1111/gcb.13824, 2018.

Fritz, M. A., Rosa, S., and Sicard, A.: Mechanisms Underlying the Environmentally Induced Plasticity of Leaf Morphology, Front Genet, 9, 478, 10.3389/fgene.2018.00478, 2018.

Fuhrer, J., Skarby, L., and Ashmore, M. R.: Critical levels for ozone effects on vegetation in Europe, Environ Pollut, 97, 91-106, 10.1016/s0269-7491(97)00067-5, 1997.

Fyllas, N. M., Quesada, C. A., and Lloyd, J.: Deriving Plant Functional Types for Amazonian forests for use in vegetation dynamics models, Perspectives in Plant Ecology, Evolution and Systematics, 14, 97-110, https://doi.org/10.1016/j.ppees.2011.11.001, 2012.

Gallagher, R. V., Falster, D. S., Maitner, B. S., Salguero-Gomez, R., Vandvik, V., Pearse, W. D., Schneider, F. D., Kattge, J., Poelen, J. H., Madin, J. S., Ankenbrand, M. J., Penone, C., Feng, X., Adams, V. M., Alroy, J., Andrew, S. C., Balk, M. A., Bland, L. M., Boyle, B. L., Bravo-Avila, C. H., Brennan, I., Carthey, A. J. R., Catullo, R., Cavazos, B. R., Conde, D. A., Chown, S. L., Fadrique, B., Gibb, H., Halbritter, A. H., Hammock, J., Hogan, J. A., Holewa, H., Hope, M., Iversen, C. M., Jochum, M., Kearney, M., Keller, A., Mabee, P., Manning, P., McCormack, L., Michaletz, S. T., Park, D. S., Perez, T. M., Pineda-Munoz, S., Ray, C. A., Rossetto, M., Sauquet, H., Sparrow, B., Spasojevic, M. J., Telford, R. J., Tobias, J. A., Violle, C., Walls, R., Weiss, K. C. B., Westoby, M., Wright, I. J., and Enquist, B. J.: Open Science principles for accelerating trait-based science across the Tree of Life, Nat Ecol Evol, 4, 294-303, 10.1038/s41559-020-1109-6, 2020.

Gelaro, R., McCarty, W., Suarez, M. J., Todling, R., Molod, A., Takacs, L., Randles, C. A., Darmenov, A., Bosilovich, M. G., Reichle, R., Wargan, K., Coy, L., Cullather, R., Draper, C., Akella, S., Buchard, V., Conaty, A., da Silva, A. M., Gu, W., Kim, G.-K., Koster, R., Lucchesi, R., Merkova, D., Nielsen, J. E., Partyka, G., Pawson, S., Putman, W., Rienecker, M., Schubert, S. D., Sienkiewicz, M., and Zhao, B.: The Modern-Era Retrospective Analysis for Research and Applications, Version 2 (MERRA-2), J Climate, 30, 5419-5454, 10.1175/jcli-d-16-0758.1, 2017.

Gong, C., Lei, Y., Ma, Y., Yue, X., and Liao, H.: Ozone–vegetation feedback through dry deposition and isoprene emissions in a global chemistry–carbon–climate model, Atmos. Chem. Phys., 20, 3841-3857, 10.5194/acp-20-3841-2020, 2020.

Gong, C., Liao, H., Yue, X., Ma, Y., and Lei, Y.: Impacts of Ozone-Vegetation Interactions on Ozone Pollution Episodes in North China and the Yangtze River Delta, Geophys Res Lett, 48, 10.1029/2021gl093814, 2021.

Henry, C., John, G. P., Pan, R., Bartlett, M. K., Fletcher, L. R., Scoffoni, C., and Sack, L.: A stomatal safety-efficiency trade-off constrains responses to leaf dehydration, Nat Commun, 10, 3398, 10.1038/s41467-019-11006-1, 2019.

Herdt, R. W.: The state of food and agriculture, 2003-2004: Agricultural biotechnology: Meeting the needs of the poor?, Agricultural Economics, 32, 109-+, 10.1111/j.0169-5150.2005.t01-7-00008.x, 2005.

Hong, C., Mueller, N. D., Burney, J. A., Zhang, Y., AghaKouchak, A., Moore, F. C., Qin, Y., Tong, D., and Davis, S. J.: Impacts of ozone and climate change on yields of perennial crops in California, Nature Food, 1, 166-172, 10.1038/s43016-020-0043-8, 2020.

Kattge, J., Diaz, S., Lavorel, S., Prentice, C., Leadley, P., Bonisch, G., Garnier, E., Westoby, M., Reich, P. B., Wright, I. J., Cornelissen, J. H. C., Violle, C., Harrison, S. P., van Bodegom, P. M., Reichstein, M., Enquist, B. J., Soudzilovskaia, N. A., Ackerly, D. D., Anand, M., Atkin, O., Bahn, M., Baker, T. R., Baldocchi, D., Bekker, R., Blanco, C. C., Blonder, B., Bond, W. J., Bradstock, R., Bunker, D. E., Casanoves, F., Cavender-Bares, J., Chambers, J. Q., Chapin, F. S., Chave, J., Coomes, D., Cornwell, W. K., Craine, J. M., Dobrin, B. H., Duarte, L., Durka, W., Elser, J., Esser, G., Estiarte, M., Fagan, W. F., Fang, J., Fernandez-Mendez, F., Fidelis, A., Finegan, B., Flores, O., Ford, H., Frank, D., Freschet, G. T., Fyllas, N. M., Gallagher, R. V., Green, W. A., Gutierrez, A. G., Hickler, T., Higgins, S. I., Hodgson, J. G., Jalili, A., Jansen, S., Joly, C. A., Kerkhoff, A. J., Kirkup, D., Kitajima, K., Kleyer, M., Klotz, S., Knops, J. M. H., Kramer, K., Kuhn, I., Kurokawa, H., Laughlin, D., Lee, T. D., Leishman, M., Lens, F., Lenz, T., Lewis, S. L., Lloyd, J., Llusia, J., Louault, F., Ma, S., Mahecha, M. D., Manning, P., Massad, T., Medlyn, B. E., Messier, J., Moles, A. T., Muller, S. C., Nadrowski, K., Naeem, S., Niinemets, U., Nollert, S., Nuske, A., Ogaya, R., Oleksyn, J., Onipchenko, V. G., Onoda, Y., Ordonez, J., Overbeck, G., Ozinga, W. A., Patino, S., Paula, S., Pausas, J. G., Penuelas, J., Phillips, O. L., Pillar, V., Poorter, H., Poorter, L., Poschlod, P., Prinzing, A., Proulx, R., Rammig, A., Reinsch, S., Reu, B., Sack, L., Salgado-Negre, B., Sardans, J., Shiodera, S., Shipley, B., Siefert, A., Sosinski, E., Soussana, J. F., Swaine, E., Swenson, N., Thompson, K., Thornton, P., Waldram, M., Weiher, E., White, M., White, S., Wright, S. J., Yguel, B., Zaehle, S., Zanne, A. E., and Wirth, C.: TRY - a global database of plant traits, Global Change Biol, 17, 2905-2935, Doi 10.1111/J.1365-2486.2011.02451.X, 2011.

Keenan, T. F. and Niinemets, U.: Global leaf trait estimates biased due to plasticity in the shade, Nat Plants, 3, ARTN 16201 10.1038/nplants.2016.201, 2017.

Kochhar, S. and Gujral, S.: Abiotic and Biotic Stress, in: Plant Physiology: Theory and Applications, 2 ed., edited by: Kochhar, S. L., and Gujral, S. K., Cambridge University Press, Cambridge, 545-589, DOI: 10.1017/9781108486392.021, 2020.

Li, D., Wang, X., Zheng, H., Zhou, K., Yao, X., Tian, Y., Zhu, Y., Cao, W., and Cheng, T.: Estimation of area- and mass-based leaf nitrogen contents of wheat and rice crops from water-removed spectra using continuous wavelet analysis, Plant Methods, 14, 10.1186/s13007-018-0344-1, 2018.

Li, P., Calatayud, V., Gao, F., Uddling, J., and Feng, Z. Z.: Differences in ozone sensitivity among woody species are related to leaf morphology and antioxidant levels, Tree Physiol., 36, 1105-1116, 10.1093/treephys/tpw042, 2016.

Li, P., Feng, Z., Catalayud, V., Yuan, X., Xu, Y., and Paoletti, E.: A meta-analysis on growth, physiological, and biochemical responses of woody species to ground-level ozone highlights the role of plant functional types, Plant Cell Environ, 40, 2369-2380, 10.1111/pce.13043, 2017.

Li, S., Moller, C. A., Mitchell, N. G., Lee, D., Sacks, E. J., and Ainsworth, E. A.: Testing unified theories for ozone response in C-4 species, Global Change Biol, 28, 3379-3393, 10.1111/gcb.16108, 2022.

Lombardozzi, D., Levis, S., Bonan, G., Hess, P. G., and Sparks, J. P.: The Influence of Chronic Ozone Exposure on Global Carbon and Water Cycles, J Climate, 28, 292-305, 10.1175/Jcli-D-14-00223.1, 2015.

Massman, W. J., Musselman, R. C., and Lefohn, A. S.: A conceptual ozone dose-response model to develop a standard to protect vegetation, Atmos Environ, 34, 745-759, 10.1016/s1352-2310(99)00395-7, 2000.

Mills, G., Hayes, F., Simpson, D., Emberson, L., Norris, D., Harmens, H., and Buker, P.: Evidence of widespread effects of ozone on crops and (semi-)natural vegetation in Europe (1990-2006) in relation to AOT40-and flux-based risk maps, Global Change Biol, 17, 592-613, 10.1111/j.1365-2486.2010.02217.x, 2011.

Mills, G., Sharps, K., Simpson, D., Pleijel, H., Frei, M., Burkey, K., Emberson, L., Uddling, J., Broberg, M., Feng, Z., Kobayashi, K., and Agrawal, M.: Closing the global ozone yield gap: Quantification and cobenefits for multistress tolerance, Glob Chang Biol, 24, 4869-4893, 10.1111/gcb.14381, 2018a.

Mills, G., Sharps, K., Simpson, D., Pleijel, H., Broberg, M., Uddling, J., Jaramillo, F., Davies, W. J., Dentener, F., Van den Berg, M., Agrawal, M., Agrawal, S. B., Ainsworth, E. A., Buker, P., Emberson, L., Feng, Z. Z., Harmens, H., Hayes, F., Kobayashi, K., Paoletti, E., and Van Dingenen, R.: Ozone pollution will compromise efforts to increase global wheat production, Global Change Biol, 24, 3560-3574, 10.1111/gcb.14157, 2018b.

Moreno-Martinez, A., Camps-Valls, G., Kattge, J., Robinson, N., Reichstein, M., van Bodegom, P., Kramer, K., Cornelissen, J. H. C., Reich, P., Bahn, M., Niinemets, U., Penuelas, J., Craine, J. M., Cerabolini, B. E. L., Minden, V., Laughlin, D. C., Sack, L., Allred, B., Baraloto, C., Byun, C., Soudzilovskaia, N. A., and Running, S. W.: A methodology to derive global maps of leaf traits using remote sensing and climate data, Remote Sens Environ, 218, 69-88, 2018.

Mukherjee, A., Yadav, D. S., Agrawal, S. B., and Agrawal, M.: Ozone a persistent challenge to food security in India: Current status and policy implications, Current Opinion in Environmental Science & Health, 19, 100220, https://doi.org/10.1016/j.coesh.2020.10.008, 2021.

Oliver, R. J., Mercado, L. M., Sitch, S., Simpson, D., Medlyn, B. E., Lin, Y. S., and Folberth, G. A.: Large but decreasing effect of ozone on the European carbon sink, Biogeosciences, 15, 4245-4269, 10.5194/bg-15-4245-2018, 2018.

Ollinger, S. V., Aber, J. D., and Reich, P. B.: Simulating Ozone Effects on Forest Productivity: Interactions among Leaf-, Canopy-, and Stand-Level Processes, Ecol Appl, 7, 1237-1251, 10.2307/2641211, 1997.

Peng, J. L., Shang, B., Xu, Y. S., Feng, Z. Z., Pleijel, H., and Calatayud, V.: Ozone exposure- and flux-yield response relationships for maize, Environ Pollut, 252, 1-7, 2019.

Poorter, H., Niinemets, U., Poorter, L., Wright, I. J., and Villar, R.: Causes and consequences of variation in leaf mass per area (LMA): a meta-analysis, New Phytol, 182, 565-588, 10.1111/j.1469-8137.2009.02830.x, 2009.

Reich, P. B.: The world-wide 'fast-slow' plant economics spectrum: a traits manifesto, J Ecol, 102, 275-301, 10.1111/1365-2745.12211, 2014.

Reich, P. B. and Amundson, R. G.: AMBIENT LEVELS OF OZONE REDUCE NET PHOTOSYNTHESIS IN TREE AND CROP SPECIES, Science, 230, 566-570, 10.1126/science.230.4725.566, 1985.

Reich, P. B., Ellsworth, D. S., and Walters, M. B.: Leaf structure (specific leaf area) modulates photosynthesis-nitrogen relations: evidence from within and across species and functional groups, Funct Ecol, 12, 948-958, DOI 10.1046/j.1365-2435.1998.00274.x, 1998.

Reich, P. B., Walters, M. B., and Ellsworth, D. S.: From tropics to tundra: Global convergence in plant functioning, P Natl Acad Sci USA, 94, 13730-13734, 10.1073/pnas.94.25.13730, 1997.

Reich, P. B., Ellsworth, D. S., Walters, M. B., Vose, J. M., Gresham, C., Volin, J. C., and Bowman, W. D.: Generality of leaf trait relationships: A test across six biomes, Ecology, 80, 1955-1969, 10.1890/0012-9658(1999)080[1955:goltra]2.0.co;2, 1999.

Richards, B. L., Middleton, J. T., and Hewitt, W. B.: Air Pollution With Relation to Agronomic Crops: V. Oxidant Stipple of Grape, Agron J, 50, 559-561, 1958.

Richards, R. A.: Selectable traits to increase crop photosynthesis and yield of grain crops, J Exp Bot, 51, 447-458, 10.1093/jexbot/51.suppl_1.447, 2000.

Shang, B., Feng, Z. Z., Li, P., Yuan, X. Y., Xu, Y. S., and Calatayud, V.: Ozone exposure- and flux-based response relationships with photosynthesis, leaf morphology and biomass in two poplar clones, Sci Total Environ, 603, 185-195, 10.1016/j.scitotenv.2017.06.083, 2017.

Shipley, B., Lechowicz, M. J., Wright, I., and Reich, P. B.: Fundamental trade-offs generating the worldwide leaf economics spectrum, Ecology, 87, 535-541, 10.1890/05-1051, 2006.

Sitch, S., Cox, P. M., Collins, W. J., and Huntingford, C.: Indirect radiative forcing of climate change through ozone effects on the land-carbon sink, Nature, 448, 791-794, 10.1038/Nature06059, 2007.

Tai, A. P. K., Martin, M. V., and Heald, C. L.: Threat to future global food security from climate change and ozone air pollution, Nat Clim Change, 4, 817-821, 10.1038/nclimate2317, 2014.

Tai, A. P. K., Sadiq, M., Pang, J. Y. S., Yung, D. H. Y., and Feng, Z.: Impacts of Surface Ozone Pollution on Global Crop Yields: Comparing Different Ozone Exposure Metrics and Incorporating Co-effects of CO2, Frontiers in Sustainable Food Systems, 5, 10.3389/fsufs.2021.534616, 2021.

Tiwari, S., Grote, R., Churkina, G., and Butler, T.: Ozone damage, detoxification and the role of isoprenoids - new impetus for integrated models, Funct Plant Biol, 43, 324-336, 10.1071/fp15302, 2016.

Turnock, S. T., Wild, O., Dentener, F. J., Davila, Y., Emmons, L. K., Flemming, J., Folberth, G. A., Henze, D. K., Jonson, J. E., Keating, T. J., Kengo, S., Lin, M., Lund, M., Tilmes, S., and O'Connor, F. M.: The impact of future emission policies on tropospheric ozone using a parameterised approach, Atmos Chem Phys, 18, 8953-8978, 10.5194/acp-18-8953-2018, 2018.

Walker, A. P., Beckerman, A. P., Gu, L., Kattge, J., Cernusak, L. A., Domingues, T. F., Scales, J. C., Wohlfahrt, G., Wullschleger, S. D., and Woodward, F. I.: The relationship of leaf photosynthetic traits – Vcmax and Jmax – to leaf nitrogen, leaf phosphorus, and specific leaf area: a meta-analysis and modeling study, Ecol Evol, 4, 3218-3235, https://doi.org/10.1002/ece3.1173, 2014.

Wang, K. and Shangguan, Z.: Photosynthetic characteristics and resource utilization efficiency of maize (Zea maysL.) and millet (Setaria italicaL.) in a semi-arid hilly loess region in China, New Zeal J Crop Hort, 38, 247-254, 10.1080/01140671.2010.503987, 2010.

Wittig, V. E., Ainsworth, E. A., Naidu, S. L., Karnosky, D. F., and Long, S. P.: Quantifying the impact of current and future tropospheric ozone on tree biomass, growth, physiology and biochemistry: a quantitative meta-analysis, Global Change Biol, 15, 396-424, 2009.

Wright, I. J., Westoby, M., and Reich, P. B.: Convergence towards higher leaf mass per area in dry and nutrient-poor habitats has different consequences for leaf life span, J Ecol, 90, 534-543, 10.1046/j.1365-2745.2002.00689.x, 2002.

Wright, I. J., Reich, P. B., Cornelissen, J. H. C., Falster, D. S., Groom, P. K., Hikosaka, K., Lee, W., Lusk, C. H., Niinemets, U., Oleksyn, J., Osada, N., Poorter, H., Warton, D. I., and Westoby, M.: Modulation of leaf economic traits and trait relationships by climate, Global Ecol Biogeogr, 14, 411-421, 10.1111/j.1466-822x.2005.00172.x, 2005.

Wu, Y., Gong, W., Wang, Y., Yong, T., Yang, F., Liu, W., Wu, X., Du, J., Shu, K., Liu, J., Liu, C., and Yang, W.: Leaf area and photosynthesis of newly emerged trifoliolate leaves are regulated by mature leaves in soybean, J Plant Res, 131, 671-680, 10.1007/s10265-018-1027-8, 2018.

Yue, X. and Unger, N.: The Yale Interactive terrestrial Biosphere model version 1.0: description, evaluation and implementation into NASA GISS ModelE2, Geosci Model Dev, 8, 2399-2417, 10.5194/gmd-8-2399-2015, 2015.

Yue, X. and Unger, N.: Fire air pollution reduces global terrestrial productivity, Nat Commun, 9, 5413, 2018.

Zalles, V., Hansen, M. C., Potapov, P. V., Parker, D., Stehman, S. V., Pickens, A. H., Parente, L. L., Ferreira, L. G., Song, X.-P., Hernandez-Serna, A., and Kommareddy, I.: Rapid expansion of human impact on natural land in South America since 1985, Sci Adv, 7, eabg1620, 10.1126/sciadv.abg1620, 2021.

Zhou, S. S., Tai, A. P. K., Sun, S., Sadiq, M., Heald, C. L., and Geddes, J. A.: Coupling between surface ozone and leaf area index in a chemical transport model: strength of feedback and implications for ozone air quality and vegetation health, Atmos. Chem. Phys., 18, 14133-14148, 10.5194/acp-18-14133-2018, 2018.

Zhu, J., Tai, A. P. K., and Hung Lam Yim, S.: Effects of ozone–vegetation interactions on meteorology and air quality in China using a two-way coupled land–atmosphere model, Atmos. Chem. Phys., 22, 765-782, 10.5194/acp-22-765-2022, 2022.

Table 1. Summary of simulations.

Experiment [a]	Method	Thresholds [a] (x or y)	LMA format	LMA map	Optimal (a or a_{PFT})	Tests (a or a_{PFT})
YIBs-LMA	Mass-based	x=0.019	gridded	M2018	a=3.5 (Table 2)	five tests (a=2.5, 3, 3.5, 4, 4.5)
YIBs-LMA_PFT		x=0.019	PFT-specific	M2018	a=2.0 (Table S3)	five tests (a=2, 2.5, 3, 3.5, 4)
YIBs-LMA_T		x=0.006	gridded	M2018	a=3.0 (Table S4)	five tests (a=2, 2.5, 3, 3.5, 4)
YIBs-LMA_B2017		x=0.019	gridded	B2017	a=2.8 (Table S5)	five tests (a=2, 2.5, 2.8, 3, 3.5)
YIBs-S2007_adj	Area-based	8 values for y (Table S6)	/	/	8 values for a_{PFT} (Table S6)	40 tests (five each for 8 PFTs)

[a] Units of thresholds are nmol g^{-1} s^{-1} for x and nmol m^{-2} s^{-1} for y

[b] Units of key parameters are $nmol^{-1}$ s g for a and $nmol^{-1}$ m^2 s for a_{PFT}

Table 2. Calibrations of the YIBs-LMA [a] experiment with varied *a*.

PFT	S_O	S_S					S_S/S_O [b]				
		a=2.5	a=3.0	**a=3.5**	a=4.0	a=4.5	a=2.5	a=3.0	**a=3.5**	a=4.0	a=4.5
EBF	-0.19	-0.13	-0.16	**-0.18**	-0.21	-0.23	0.70	0.83	**0.96**	1.08	1.20
NF	-0.23	-0.26	-0.31	**-0.36**	-0.40	-0.45	1.14 *	1.35 *	**1.56** *	1.75 *	1.95 *
DBF	-0.70	-0.51	-0.60	**-0.69**	-0.78	-0.87	0.72	0.86	**0.99**	1.12	1.24
C_SHR	/	-0.75	-0.90	**-1.04**	-1.18	-1.31	/	/	/	/	/
A_SHR	/	-0.38	-0.45	**-0.53**	-0.60	-0.66	/	/	/	/	/
C4_GRA	-0.85	-0.71	-0.84	**-0.97**	-1.10	-1.22	0.83	0.99	**1.14**	1.29	1.44
C3_GRA	-0.62	-0.47	-0.55	**-0.64**	-0.73	-0.81	0.75	0.89	**1.03**	1.17	1.30
CRO	-3.35	-1.97	-2.57	**-3.28**	-4.11	-5.10	0.59	0.77	**0.98**	1.23	1.52
Fitting [c]	/	0.61	0.79	**0.99**	1.23	1.50	/	/	/	/	/
Median	/	/	/	/	/	/	0.74 (0.72)	0.88 (0.86)	**1.01** **(0.99)**	1.20 (1.17)	1.37 (1.30)
Std	/	/	/	/	/	/	0.19 (0.09)	0.21 (0.08)	**0.23** **(0.07)**	0.25 (0.08)	0.28 (0.13)

[a] All runs from the YIBs-LMA experiment use x=0.019 nmol g^{-1} s^{-1} and LMA map from M2018.

[b] Slopes of simulated DRRs (S_S) are divided by observations (S_O, Table S1) to derive the model-to-observation ratios ("S_S/S_O"). O_3 dose metric is $POD_{y=1}$ for natural PFTs and $POD_{y=6}$ for crops. The Median and standard deviation (Std) of S_S/S_O ratios of all PFTs are calculated for each set of specific parameter *a*. The values in parentheses exclude the effect of those numbers marked with * that are out of 1 standard deviation.

[c] The slopes (Fitting) of linear regressions between S_O and S_S are listed for each *a*. The optimal *a* with 1:1 fitting between S_S and S_O is bolded.

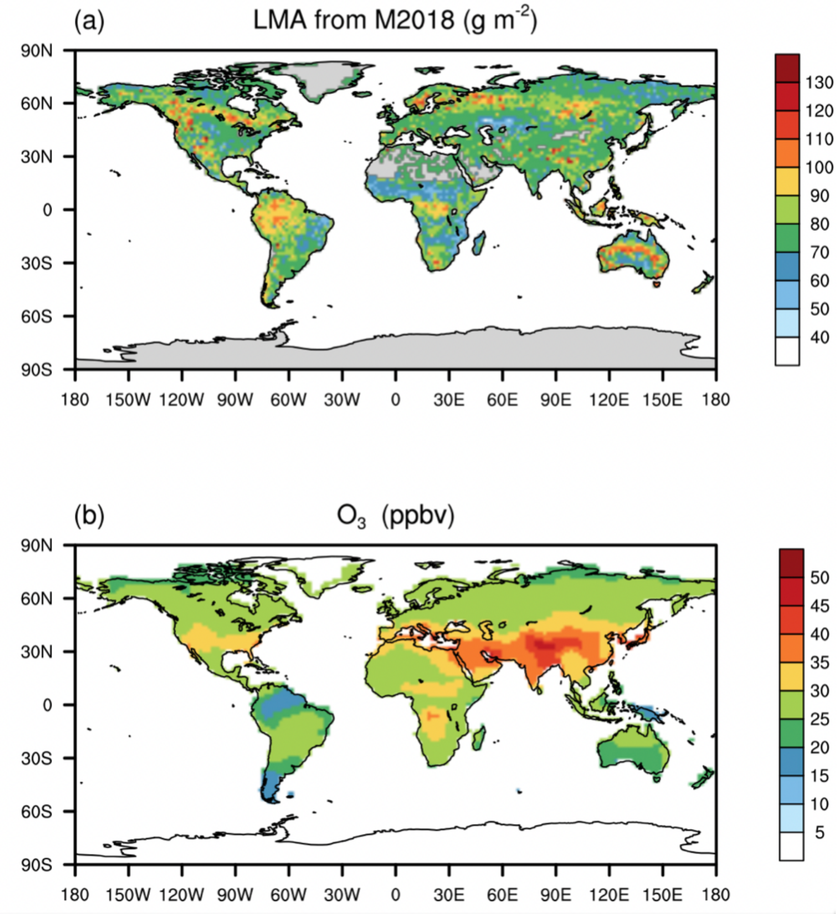

Figure 1. Global leaf mass per area (LMA) and surface ozone (O_3) concentrations. The (a) LMA is adopted from Moreno-Martinez et al. (2018) (M2018) and (b) annual mean O_3 is derived from TF-HTAP (Turnock et al., 2018).

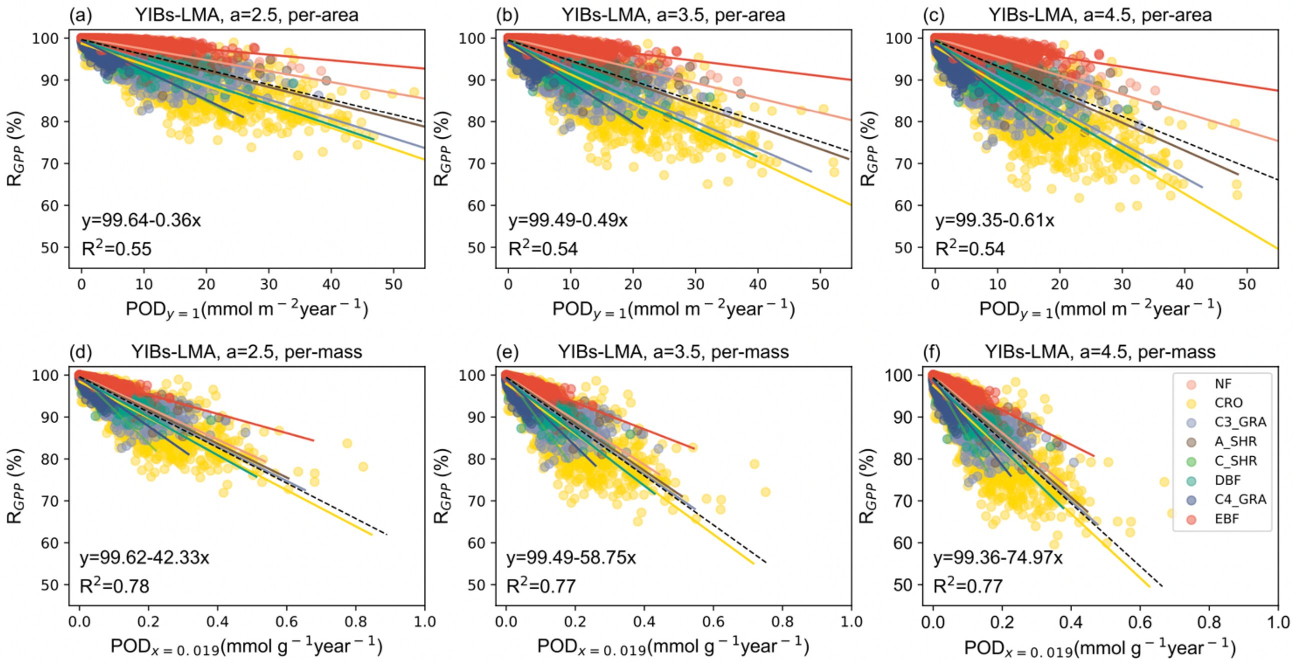

Figure 2. Simulated area-based (top) or mass-based (bottom) DRRs for the YIBs-LMA experiment. Three tests from the YIBs-LMA experiment all adopt *x*=0.019 nmol g^{-1} s^{-1} and gridded LMA from M2018 with parameter *a*=2.5, 3.5, 4.5 nmol^{-1} s g, respectively. Each dot represents estimated POD-R_{GPP} ($POD_{y=1}$ for (a)-(c), $POD_{x=0.019}$ for (d)-(e)) at a grid with corresponding PFT. The PFT-specific regressions between area- or mass- based POD and R_{GPP} are displayed with solid lines shown in legend. Regression relationships of all PFTs are displayed in black dash line with coefficients of determination (R^2) denoted on each panel. Note the differences of ranges in x axis among PFTs. The YIBs-LMA experiment is summarized in Table 1.

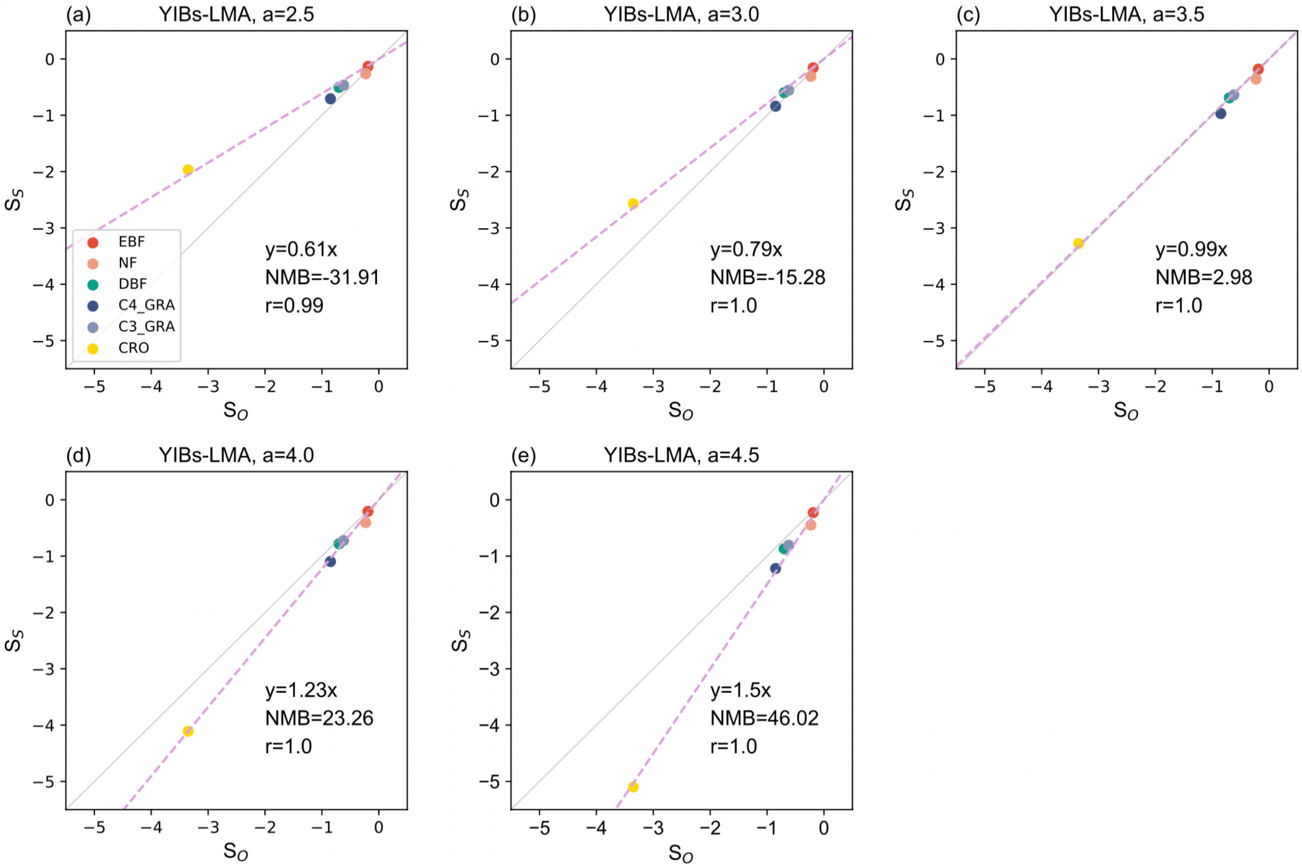

Figure 3. Comparison between S_O (% per mmol m^{-2}) and S_S (% per mmol m^{-2}) for the YIBs-LMA experiment. Five tests from the YIBs-LMA experiment all adopt x=0.019 nmol g^{-1} s^{-1} and gridded LMA from M2018 but with varied parameter a from (a) 2.5 to (e) 4.5 nmol^{-1} s g. S_O are from Table S1. S_S are derived as the slope between R_{GPP} and POD_y. The linear regression (dashed lines), 1:1 fitting (light grey lines), normalized mean biases (NMB), and correlation coefficient (r) between S_S and S_O for varied PFTs are shown on each panel. The S_S and S_O of CRO are derived using $POD_{y=6}$ while other PFTs use $POD_{y=1}$. The YIBs-LMA experiment is described in Table 1.

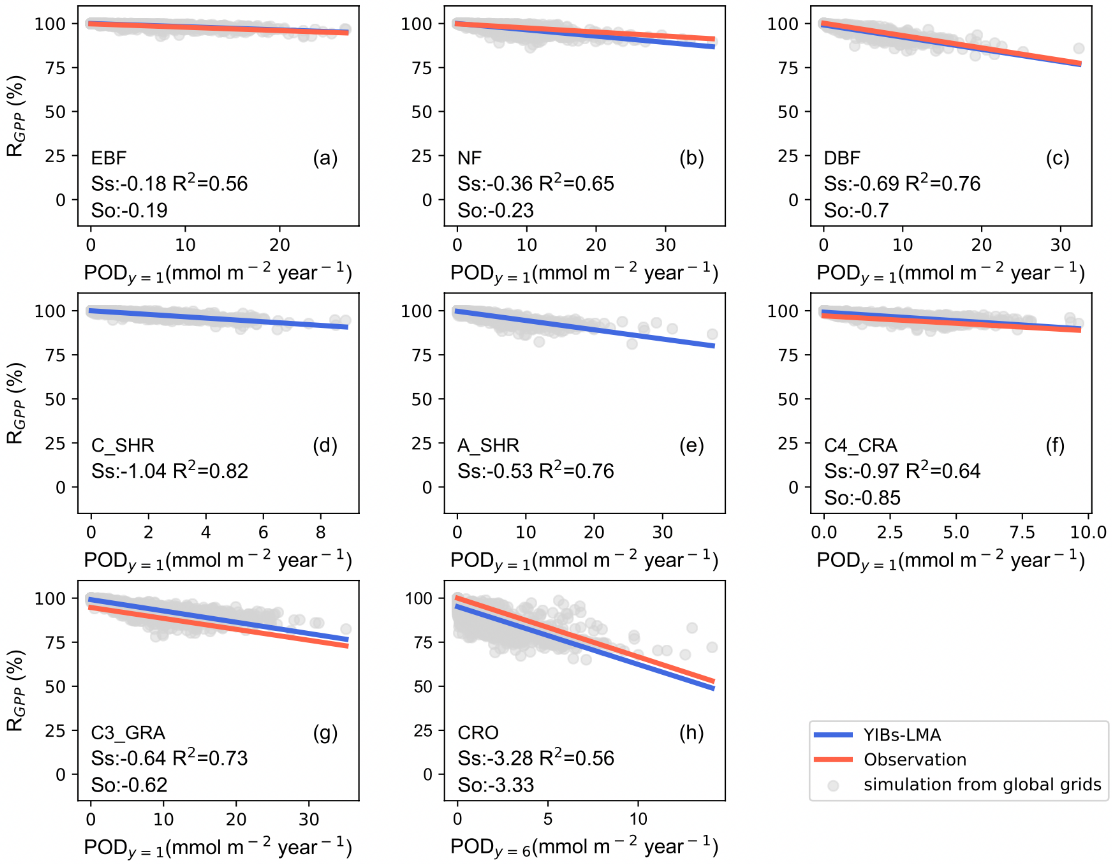

Figure 4. Comparisons of observed and simulated dose-response relationships. Simulated PFT-specific DRRs are derived from YIBs-LMA with gridded LMA from M2018, *x*=0.019 nmol g^{-1} s^{-1}, and *a*=3.5 $nmol^{-1}$ s g. Each dot represents results from a gridcell with corresponding PFT. The regressions between relative GPP percentage (R_{GPP}) and leaf area-based stomatal O_3 uptake fluxes ($POD_{y=1}$ for natural PFTs and $POD_{y=6}$ for crops) are shown for observations (red, see Table S1) and simulations (blue) with slopes of DRRs denoted as *So* and *Ss*, respectively. S_O are missing for (d) cold and (e) arid shrubs. Coefficients of determination (R^2) of simulations are displayed in each panel. Note the differences of ranges in x axis among PFTs (PFTs are shown in Fig. S1).

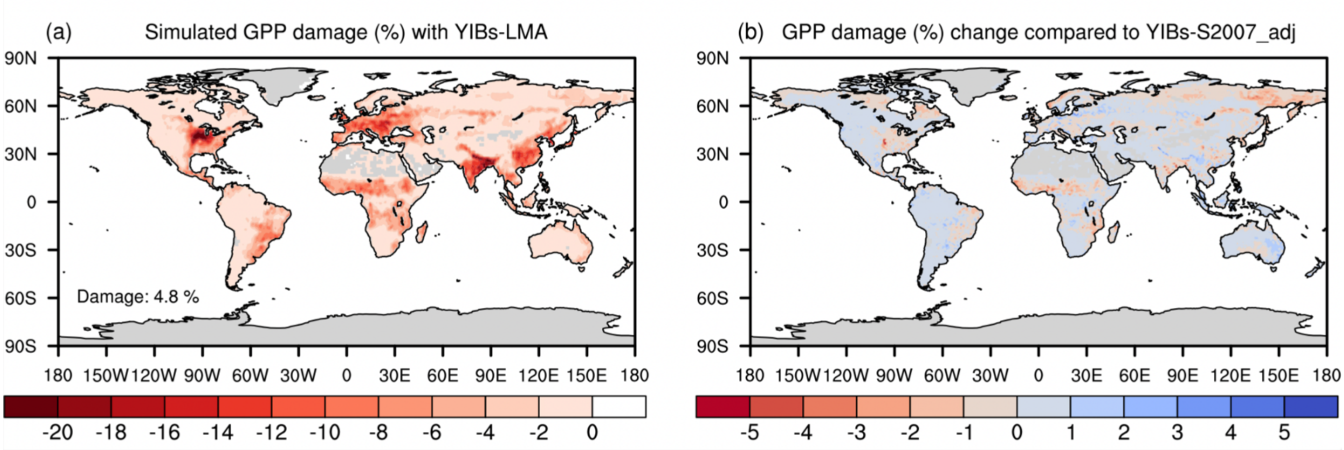

Figure 5. Global O_3 vegetation damage simulated with the LMA-based scheme. Results shown are the (a) GPP reduction percentages by O_3 simulated with the YIBs-LMA framework (gridded LMA from M2018, x=0.019 nmol g^{-1} s^{-1}, and a=3.5 nmol^{-1} s g), and (b) their differences compared to the predictions from YIBs-S2007_adj simulation. Blue (red) patches indicate the regions where damages predicted in YIBs-LMA are lower (higher) than those in YIBs-S2007_adj.

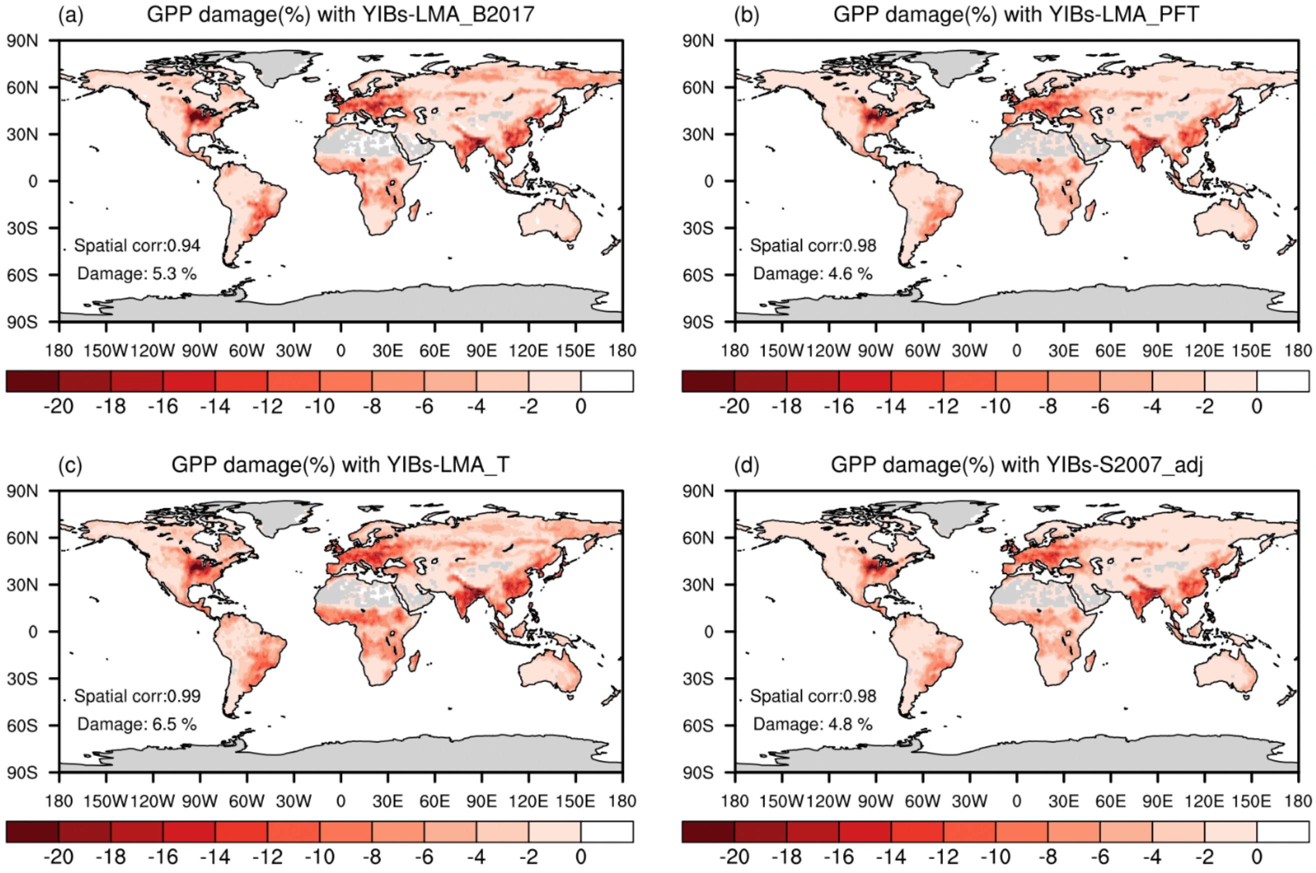

Figure 6. Global O$_3$-induced GPP reductions simulated in four supporting experiments. All damage maps are based on optimal parameters shown in Table 1. The spatial correlation coefficients between YIBs-LMA and these supporting simulations are shown on each panel as well as the global average damage percentage of each map. Simulations are described in Table 1.

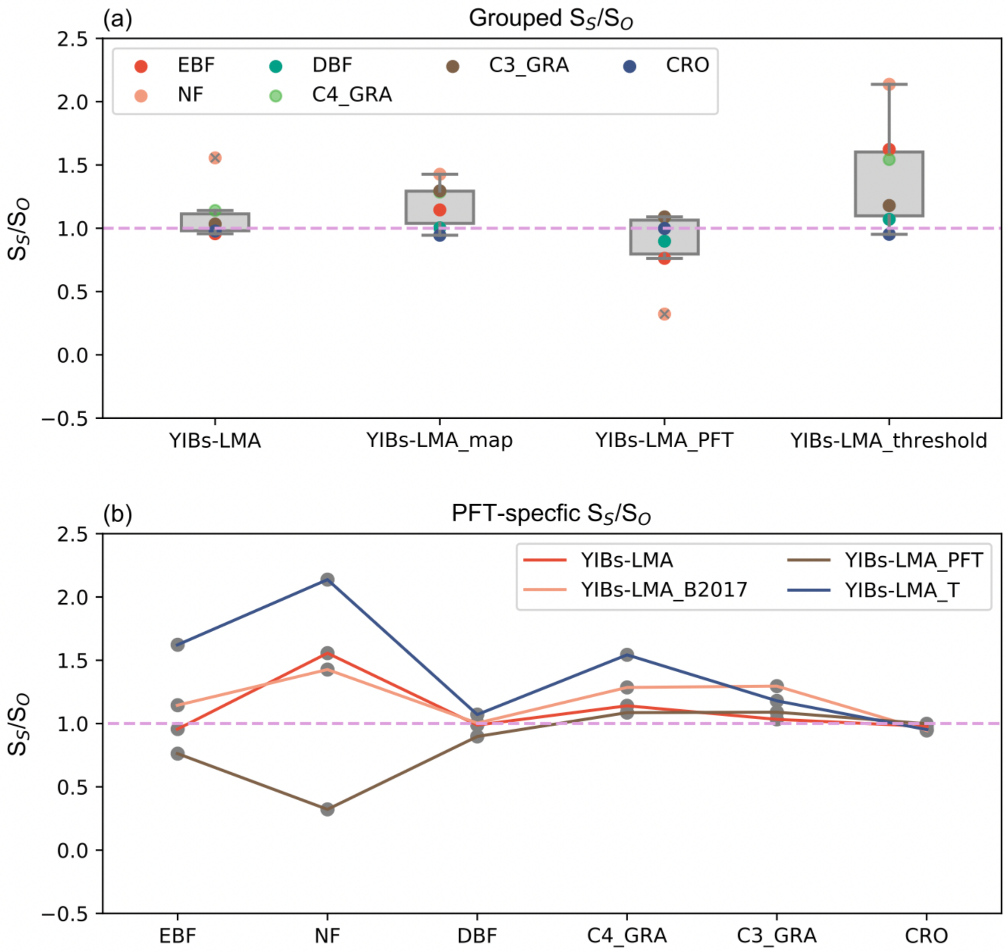

Figure 7. Comparison of S_S/S_O among supporting experiments. Individual ratios for (b) different PFTs are grouped to the boxplot in (a). All experiments adopt optimal parameters shown in Table 1.

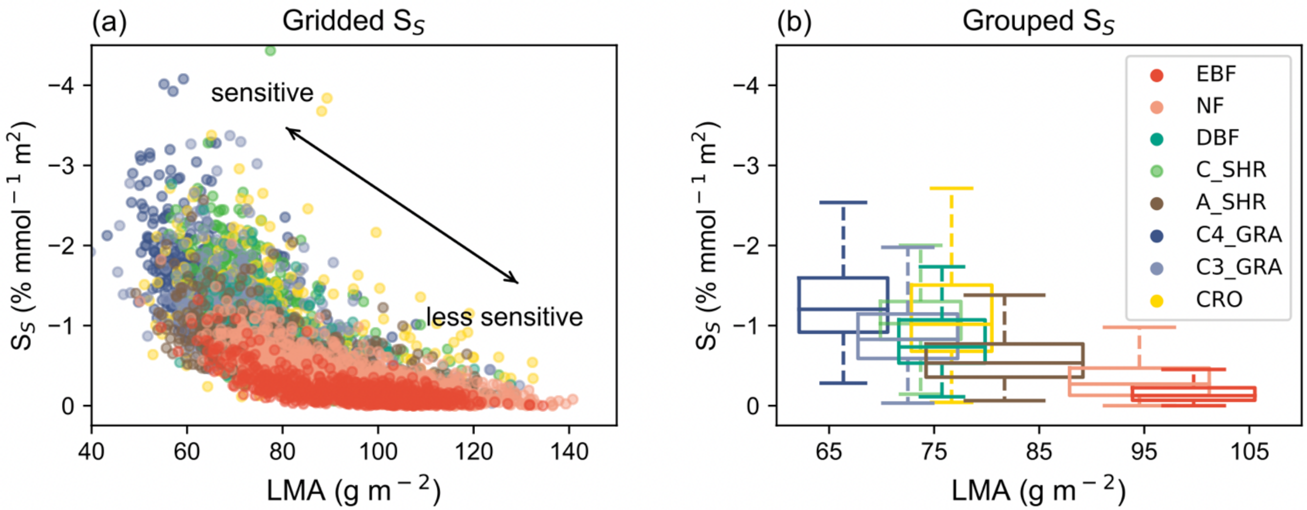

Figure 8. Relationships between O_3 sensitivity and LMA. (a) Simulated O_3 sensitivity (S_S) at each grid is compared with LMA for different PFTs. Gridded S_S is derived as GPP change per unit $POD_{y=1}$ from the YIBs-LMA simulation. Each point represents the value in a grid cell with a dominant PFT. (b) The PFT-level relationships between LMA and O_3 sensitivity are grouped as boxplots, which indicate the median, 25th percentile, and 75th percentile of y-axis variables within the same PFT. The width of boxplots represents one standard deviation of LMA for a specific PFT.

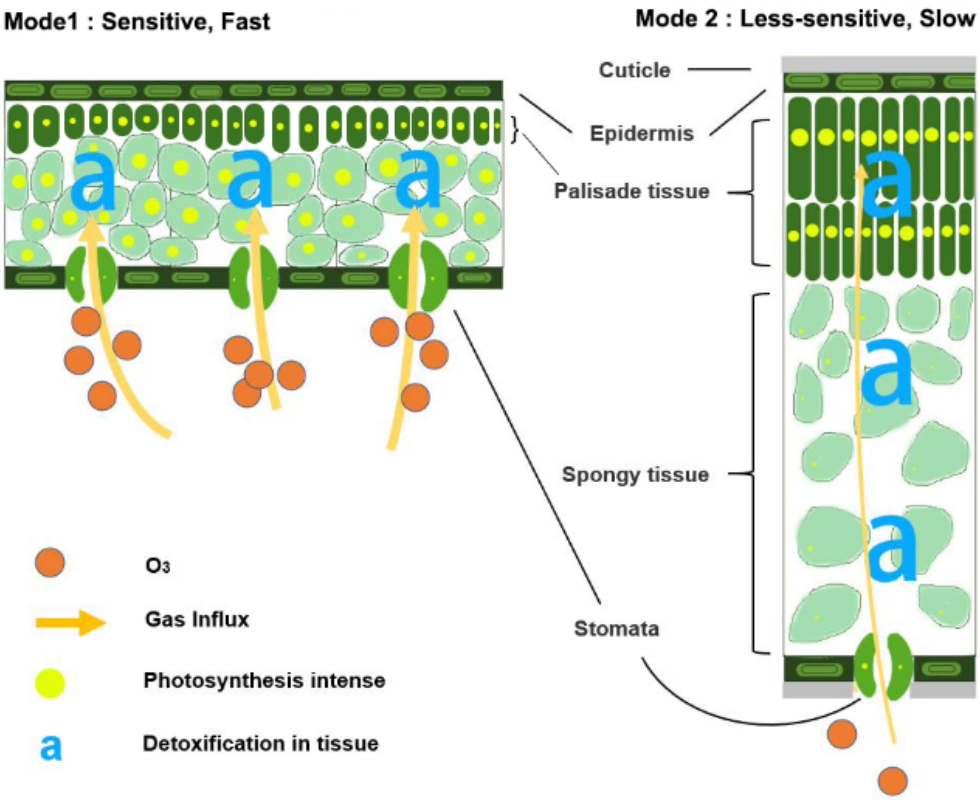

Figure 9. Illustration of the relationships between leaf trade-off strategy and its sensitivity to O_3